J. Eur. Opt. Society-Rapid Publ. 2023, **19**, 7

https://doi.org/10.1051/jeos/2023004
Available online at: https://jeos.edpsciences.org

Journal of the European Optical Society-Rapid Publications

EOSAM 2021

RESEARCH ARTICLE OPEN ACCESS

Wide band UV/Vis/NIR blazed-binary reflective gratings for spectro-imagers: two lithographic technologies investigation

Mane-Si Laure Lee[1,*], Julie Cholet[1], Anne Delboulbé[1], Raphaël Guillemet[1], Brigitte Loiseaux[1], Patrick Garabédian[1], Thomas Flügel-Paul[2], Tino Benkenstein[2], Susann Sadlowski[2], Nicolas Tetaz[3], Roman Windpassinger[4], and Ana Baselga Mateo[4]

[1] Thales Research & Technology, 1 Avenue Augustin Fresnel, 91767 Palaiseau, France
[2] Fraunhofer Institute for Applied Optics and Precision Engineering, Albert-Einstein-Strasse 7, 07745 Jena, Germany
[3] Thales Alenia Space, 5 Allée des Gabians, BP 99, 06156 Cannes la Bocca Cedex, France
[4] European Space Research and Technology Centre, Postbus 299, 2200 AG Noordwijk, The Netherlands

Received: 1 February 2022 / Accepted: 10 January 2023

Abstract. We report on subwavelength reflective gratings for hyperspectral applications operating in a very large spectral band (340–1040 nm). Our study concerns a blazed-binary grating having a period of 30 µm and composed of 2D subwavelength structures with size from 120 nm to 350 nm. We demonstrate the manufacturing of the gratings on 3″ wafers by two lithography technologies (e-beam and nanoimprint) followed by classical dry etching process. Optical measurements show that the subwavelength grating approach enables a broadband efficiency, polarization behaviour and wavefront quality improvement with respect to the requirements for the next generation of spectro-imagers for Earth observation missions. An outlook towards spherical substrate based on nanoimprint lithography is also reported with the results of mixed features replication (holes and pillars in the range of 160–330 nm) on a 540 mm concave substrate which demonstrate uniformity and accuracy capabilities over 3″ surface.

Keywords: Diffraction grating, Subwavelength structures, Electron beam lithography, Nanoimprint lithography, Effective index media.

1 Introduction

Next generation of spectro-imagers for future Earth observation missions requests ultra-wide band operation, very large field of view but small volume. However, the performance of these future instruments is limited by the performance of the diffraction grating, since high diffraction efficiency and reduced polarization sensitivity over wide spectral range are required, while introducing a limited wavefront error (WFE). In this paper, we report on gratings with period of 30 µm and operating at an angle of incidence of 0.5°, matching the specific requirements of a Dyson spectrometer [1]. The required minimum throughput lies between 35% and 50% but must be achieved within 340–1040 nm spectral range.

Classical continuous reflective saw-tooth profile blazed-gratings offer peak efficiencies up to ~90% (mainly limited by the reflectivity of the metallic material) but it decreases significantly when approaching the band edges in the ultraviolet (UV) and near-infrared (NIR) regions. To overcome this limited spectral efficiency, several approaches have been proposed in the literature. The first approach consists of combining several materials to achromatize the efficiency. Originally proposed for transmission gratings [2, 3], it has been applied recently to reflection gratings [4]. Another alternative is the so-called "multi-blaze" or "multi-angle" approach [5, 6]. Different sawtooth depths or different facet angles are combined within the same grating.

A third type of approach is based on blazed-binary gratings composed of subwavelength structures [7–9] and effective index dispersion engineering.

Here, we evaluate the optical performance of blazed-binary gratings manufactured by two lithography techniques: e-beam and nanoimprint lithography (NIL) and compare their performance with next generation spectro-imager requirements, which are summarized in Table 1.

E-beam lithography has shown its ability for the manufacturing of transmission type blazed-binary gratings for the Gaia Space Mission [10]. However, many spectrometer designs are based on the application of gratings in reflection. The gratings described in this paper relate to the

* Corresponding author: mane-si-laure.lee@thalesgroup.com

Table 1. Grating requirements related to UV/Vis/NIR spectro-imager.

Spectral band	340–1040 nm
Diffraction efficiency in the −1st diffraction order	λ = 340 nm: >0.5 λ = 440 nm: >0.4 λ = 800 nm: >0.35 λ = 1040 nm: >0.35
Polarization sensitivity	<10% (goal < 1%)
Spectral ghosts intensities	<1e−4 (with respect to useful diffracted order)
Wavefront error	WFE < 100 nm RMS

demand for a concave blazed grating of a Dyson spectrometer.

NIL is a less mature technology, as compared to e-beam lithography. However, the progress of the NIL equipment and process enables now the patterning of very small resolution features. As a replication technology, NIL enables fast and cost-effective manufacturing process fitted for low/medium-volume for earth observation missions.

2 Subwavelength gratings fabrication

The design of blazed-binary subwavelength gratings is based on artificial distributed-index media engineering [11] and purposeful design of size, shape and arrangement of the subwavelength features for tailoring the grating's spectral characteristics. The 30 µm grating period is composed of 2D subwavelength binary structures with sizes from 120 nm to 350 nm and depth of ~510 nm.

The gratings realization uses the same process steps, except for the lithography step. The process flow is depicted in Figure 1.

We use a lithography step to define the patterns into a resist layer, followed by dry etching processes to i) transfer the patterns into the metal mask and ii) to transfer the patterns into the underlying SiO_2 material and get high aspect ratio structures.

Regarding the lithography step, two techniques were investigated: 1) e-beam lithography at Fraunhofer Institute for Applied Optics and Precision Engineering (IOF), which is the most common technique to tackle such small size patterns and 2) NIL at Thales Research & Technology (TRT). The NIL is a replication technology which consists of fabricating a transparent polymer stamp (polydimethylsiloxane PDMS) and applying the stamp onto a photosensitive resist layer cured under UV light. The polymer stamp which is illustrated in Figure 2 is previously produced from a flat silicon master mold fabricated with e-beam lithography (at IOF). Thanks to a Surface Conformal Imprint Lithography module from Süss MicroTec, one stamp enables several replications with a high reproducibility and homogeneous patterning over 3″ surface.

The advantage of NIL enables the same high resolution as e-beam lithography, with reduced process time (typically few minutes per wafer *vs.* few hours). Pictures of two gratings are given in Figure 3.

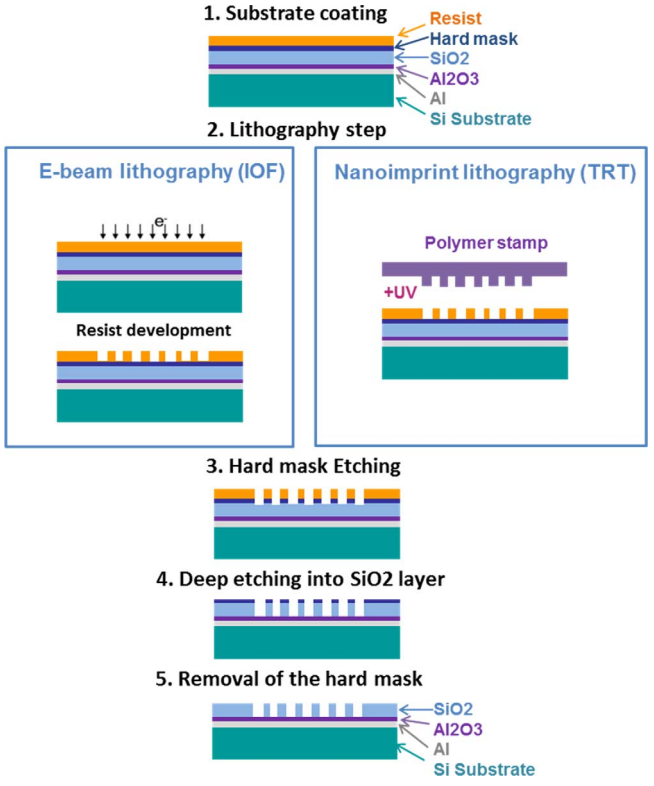

Fig. 1. Process flow for the realization of the blazed-binary gratings.

3 Optical measurements

The ~80 mm diameter blazed-binary subwavelength gratings were characterized optically at IOF premises.

The efficiency measurements were performed using a tunable light source. The gratings are illuminated by a monochromatic light beam (diameter: ~3 mm) with adaptable wavelength (FWHM < 5 nm). Measurements are carried out under transverse electric (TE) and transverse magnetic (TM) polarization. The diffracted light is detected using an integrating sphere which is mounted on a goniometer setup.

Figure 4 shows efficiency maps at 376 nm, 600 nm and 1000 nm for the subwavelength grating by e-beam lithography. The mapping sampling is 4 mm × 4 mm. It shows the large-scale uniformity of the manufactured grating.

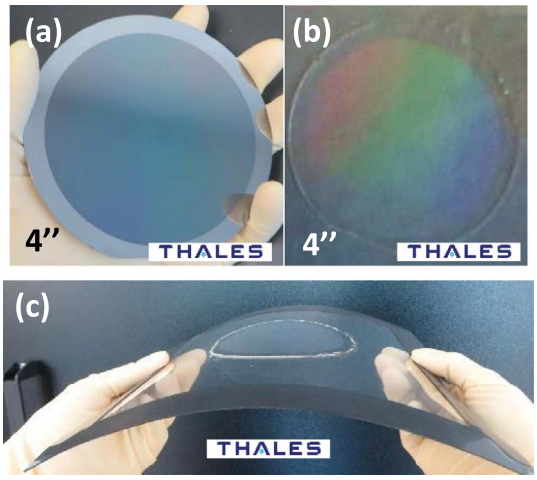

Fig. 2. Silicon master (4″) (a) and manufactured PDMS mold (b) fixed on a thin glass plate (c) used for the NIL grating manufacturing.

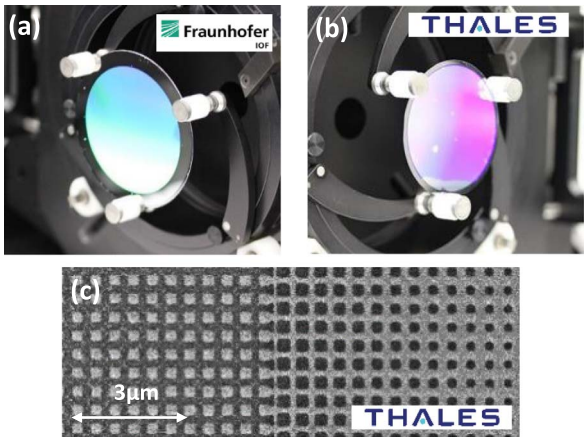

Fig. 3. Manufactured gratings on 4″ wafer by e-beam lithography (a) and on 3″ wafer by NIL (b). (c) SEM top view of few subwavelength structures of the NIL grating.

Figure 5 illustrates the −1st order reflective efficiency of the gratings illuminated under unpolarized light and at 1° angle of incidence. The black line corresponds to the e-beam grating, as compared to the green line (design efficiency), and the red line (requirement). The blue line corresponds to the NIL grating with a 50 nm depth deviation with respect to the nominal depth.

From Figure 5, two main results are straightforward.

- First, both e-beam and NIL give similar efficiency behavior which is in average 10–20% above the requirement (red line).
- Secondly, the proposed design (green line) and subwavelength grating technology (black and blue line) are tolerant to height deviation of 50 nm (blue line) and efficiency remains compatible with requirements.

Figure 6 illustrates the −1st order reflective efficiency polarization sensitivity of the gratings under TE and TM polarization. From TE and TM efficiency measurements, we calculated the polarization sensitivity, defined as

$$|\eta_{\mathrm{TE}} - \eta_{\mathrm{TM}}|/(\eta_{\mathrm{TE}} + \eta_{\mathrm{TM}}), \quad (1)$$

where η_{TE} and η_{TM} correspond to efficiencies measured under TE and TM polarized light.

It results that the polarization sensitivity is smaller than 2% for both gratings over the whole spectral band, which confirms experimentally subwavelength optics polarization property.

E-beam technology is well-known for its ability to achieve low level grating ghosts [12]. To verify this property for the NIL grating, we carried out angular scanning of many diffraction orders in the diffraction plane and plot the efficiency (power/reference) on the y-axis as a function of the detector angle θ on the x-axis (see Fig. 7).

The diffracted orders are separated by $\Delta\theta \approx 1.3°$ and the −1st order is located at $\theta = -6.3°$. It results that no additional peak is visible, meaning that no grating ghosts are measured. Note that this result is not surprising as the NIL technology uses a master based on e-beam lithography. However, it shows that the NIL technology does not introduce additional ghosts.

The wavefront error (WFE) introduced by the fabrication process is evaluated by measuring the reflected WFE of the gratings, using a plane-wave Zygo Verifire AT 12″ interferometer at a wavelength of 633 nm.

The wavefront deformation introduced by the fabrication process is evaluated as follows: 1) the retro-reflected wavefront of the grating is measured for collimated illumination obeying Littrow condition. A first measurement is performed in +1st diffraction order and a second measurement is independently performed in −1st diffraction order. 2) Both wavefront maps are then subtracted. This allows removing the influence of the grating substrate's deformation. The result only covers the inaccuracy introduced by the respective patterning process (see Fig. 8).

For both technologies, the WFE is smaller than 20 nm RMS, which is 5 times smaller than the 100 nm RMS space application requirement.

To our knowledge, although NIL technology is less mature than e-beam lithography, it is the first time that such excellent WFE over 3″ size component is measured.

4 Outlook towards curved substrates

The next generation of hyperspectral imagers will need to operate over very wide spectral bands and large fields of view, while being very compact and lightweight. For this purpose, architectures using a spherical grating such as Offner or Dyson type are of interest. So it is important to investigate the routes towards manufacturing blazed-binary gratings on spherical substrate.

Several approaches have been proposed for echelette-type spherical gratings fabrication. One approach is based on "multi-zone" e-beam writing for the fabrication of a convex (radius of 88 mm) echelette grating operating in 400 nm–1 µm [13, 14]. Another approach is based on

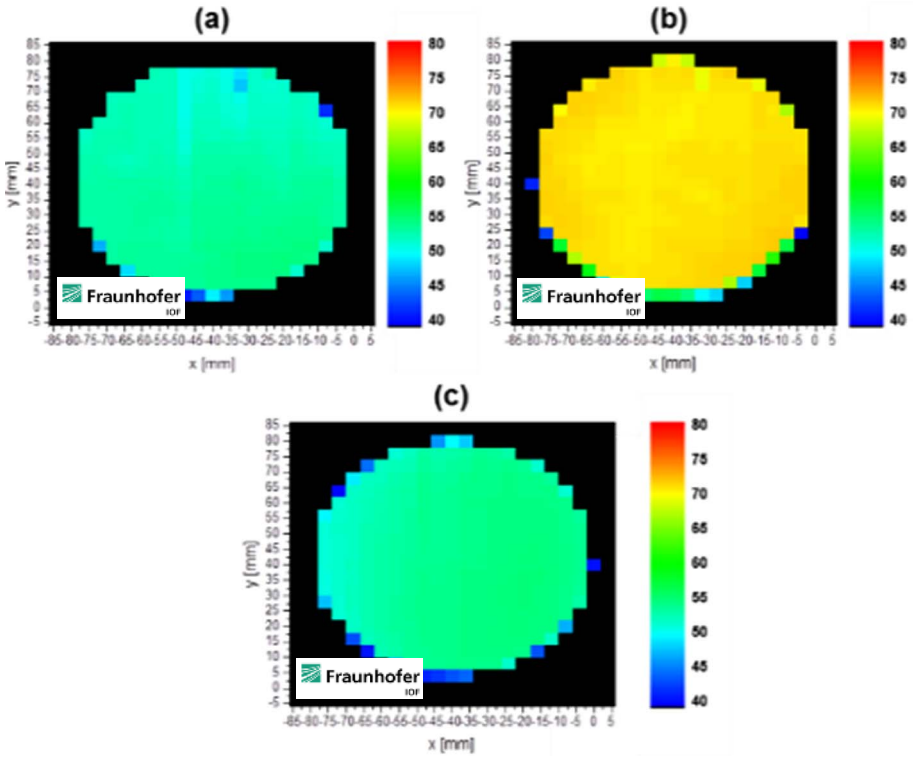

Fig. 4. Spatial mapping of the diffraction efficiency in −1st order of the prototype flat grating for three different wavelengths, i.e. 376 nm (a), 600 nm (b) and 1000 nm (c).

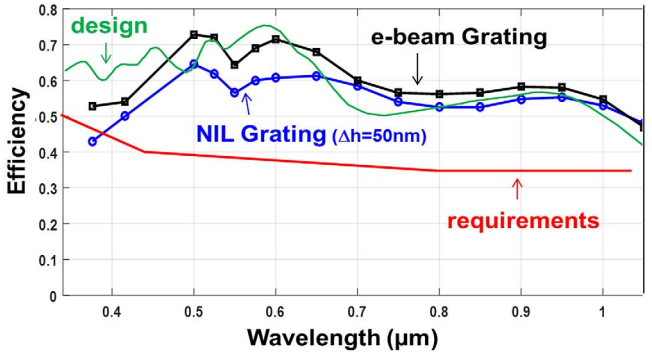

Fig. 5. Measured −1st order diffraction efficiency of blazed-binary subwavelength gratings.

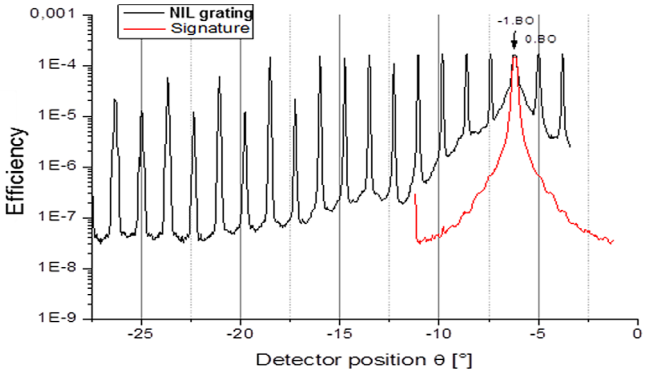

Fig. 7. Angular scanning of the efficiency in the diffractive plane at 633 nm for the NIL blazed-binary grating.

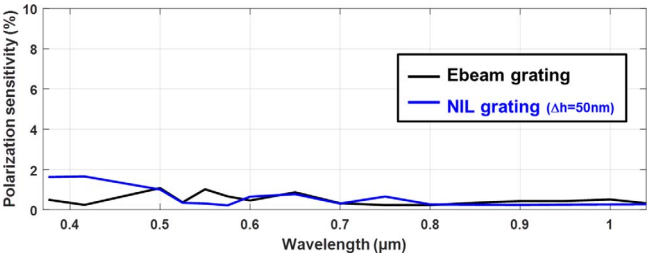

Fig. 6. Polarization sensitivity of the blazed-binary subwavelength gratings.

nanoimprint lithography on a spherical substrate and transfer onto/into the substrate for the realisation of a convex (radius of 225 mm) echelette grating of 3.3 µm period for operation in 400–800 nm [15].

To go towards spherical substrates for blazed-binary subwavelength gratings, two approaches, depicted in Figure 9 have been identified for concave substrate with a radius of curvature of the order of 500 mm. The first approach, based on a bonding approach, consists in manufacturing a full grating on a wafer substrate followed by thinning the wafer to have it enough flexible and bonding

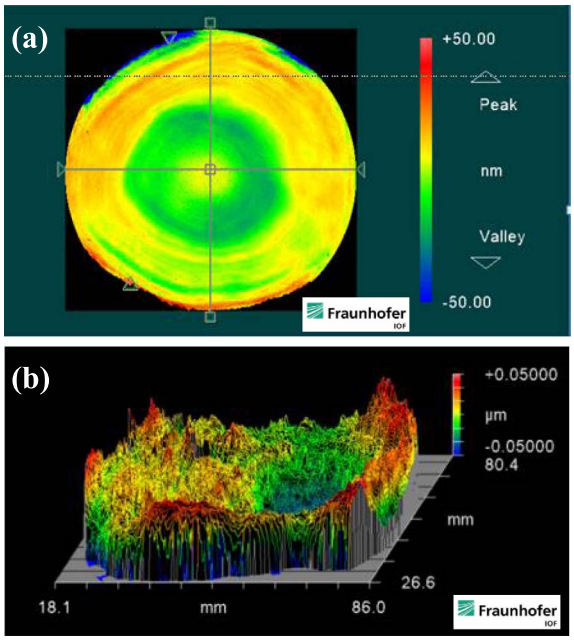

Fig. 8. Reflected wavefront introduced by the grating fabrication process (excluding substrate deformation) for e-beam grating (a) and for NIL grating (b).

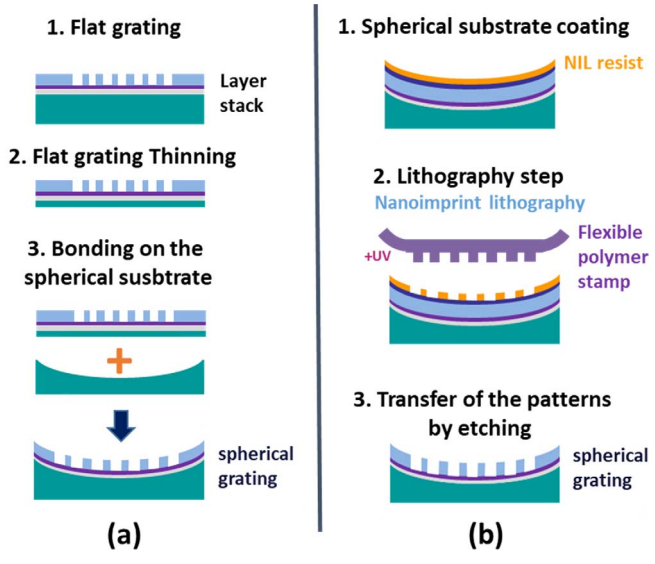

Fig. 9. Two identified routes for blazed-binary subwavelength grating fabrication on spherical substrate. (a) Thinning and bonding of a flat grating on a spherical substrate. (b) NIL on spherical substrate.

it on the spherical substrate (Fig. 9a). Bonding on plane surface has been reported for manufacturing of grism [16, 17] but should be investigated for subwavelength gratings and adjusted for non-planar substrate. The second approach consists in taking benefit of the flexibility of the nanoimprint stamp to perform a replication on curved gratings before the transfer of the patterns (Fig. 9b).

In this paper, we focus on the second approach. The first step to validate is the lithography step, i.e. the use of NIL

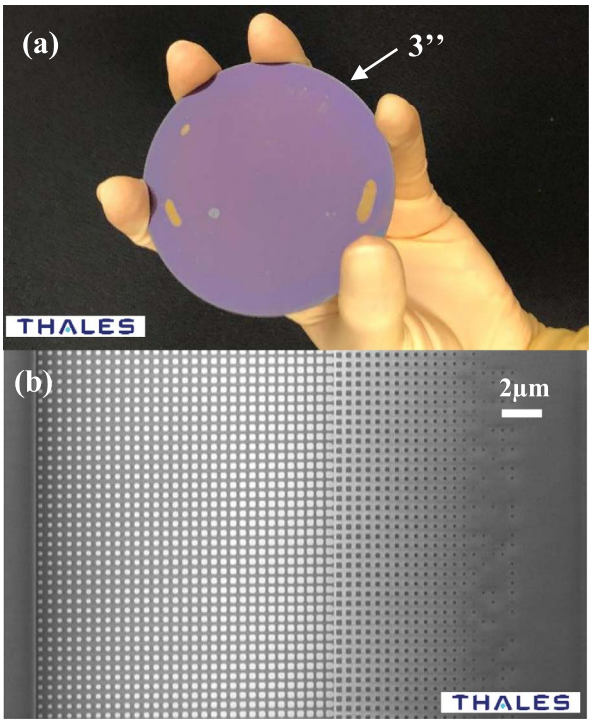

Fig. 10. Preliminary NIL replication tests on concave (R = 540 mm) substrate. (a) Picture of the 3″ resist patterned area. (b) Scanning electron microscope photograph of the grating pattern (in resist layer).

on spherical substrate. We present hereafter preliminary replication tests to validate the use of NIL on spherical substrate, by controlling the geometry of the replicated pattern and its uniformity over the spherical substrate. For this purpose, we first applied the PDMS flexible stamp into a resist layer coated on a 3″ 540 mm-radius concave silica substrate, with a home-made equipment. The resist is then exposed to UV illumination and the stamp pattern is transferred into the resist layer, step 2 in Figure 9b. Then we measured the replicated structures dimensions over the substrate.

Figure 10a shows the 3″ concave substrate after NIL replication on the resist layer (Fig. 9b step 2). The component looks homogeneous apart from small zones.

Figure 10b, taken by a scanning electron microscope (SEM), shows nice details of the resist pattern achieved on the concave substrate. This resist pattern is composed of both pillars and holes with size ranging from 160 nm to 330 nm.

The challenge for nanoimprint technology on spherical substrate is to ensure a homogeneous pressure over the substrate to achieve the suitable uniformity of the pattern dimension uniformity. To check the pattern uniformity, we have measured the pillars and holes widths from SEM photographs taken within five zones of the substrate. Figure 11 represents the location of the measurements zones (O, A, B, C, D).

To quantify the uniformity, we have measured the holes and pillars width dispersion on five zones with respect to the average width over the five zones. In total, we have

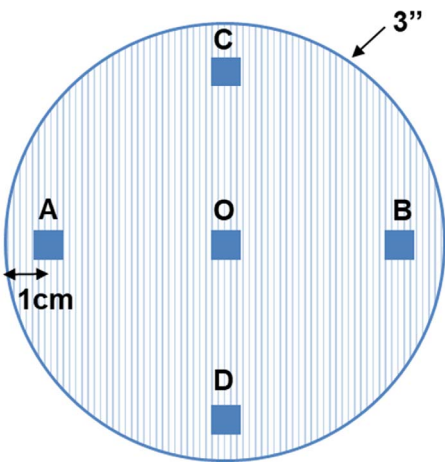

Fig. 11. Location of the measurements zones, within the substrate.

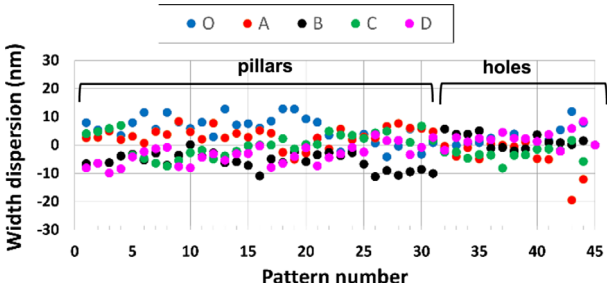

Fig. 12. Measured width dispersion of the replicated patterns on different zones of the 3″ concave substrate. Horizontal axis corresponds to the number of the patterns. Each series of points corresponds to the zones of Figure 11.

proceeded to the measurements for 44 different geometries included into one period of the grating: 31 pillars having widths varying between 180 nm to 330 nm and 13 holes having widths varying between 160 nm and 330 nm are measured. For each geometry, the measured width is the average of six measurements.

Figure 12 plots the width dispersion (with respect to the average width on five zones) for different geometries composing the grating resist pattern. These patterns are numbered from 1 to 44 along horizontal axis.

From the graph of Figure 12, we measured a variation of the pattern size within the concave 3″ substrate surface that is smaller ±20 nm for the 44 different patterns and for the 5 zones. This variation is small and is in the order of magnitude of the measurements accuracy using SEM. It shows that our preliminary test of replication on a 540 mm concave substrate is promising.

The optimization of the process to ensure a good uniformity is still under investigation and constitutes the main manufacturing challenge for the next generation of gratings.

5 Conclusion and perspectives

We have studied and characterized wide spectral band and large area 3″ blazed-binary subwavelength reflective gratings based on a same design that have been manufactured by two technologies: e-beam lithography and NIL. They are composed of high aspect ratio (~5), high density and one level subwavelength binary structures.

Optical measurements show that the subwavelength blazed-binary gratings approach and manufacturing processes based on either e-beam or nanoimprint technologies are very promising for space application. They enable superior performance, in term of spectral band (efficiency margin of 10–20% in average), polarization sensitivity (<2%), very low ghost level (not detectable), and WFE level (<20 nm RMS) with respect to requirements for observation spectro-imagers operating in UV/Vis/NIR.

As next step will be to address the grating manufacturing on spherical substrate to enable more performant spectro-imager architectures, we also investigated the challenge of nanoimprint on spherical substrate. Results of nanoimprint replication done on a 540 mm-radius concave substrate show that NIL technology enable uniformity better than ±20 nm over the 3″ surface. Such result obtained for large radius of curvature (~500 mm) are very promising as the main challenge is related to uniform application of the flexible stamp with a homogeneous pressure over the spherical substrate. This is the first time to our knowledge that such experimental demonstration and measurements, based on NIL replication of high density pattern, composed of mixed pillars and holes with different size ranging from 160 nm to 330 nm, arranged on a 500 nm grid, and on a 3″ concave substrate, are reported.

Acknowledgments. Part of this work was carried out within the framework of the ESA TRP project “Wide band and high efficiency reflective grating”, No 4000118037/16/NL/PS.

Authors would like to thanks Thierry Viard for fruitful discussion and early identification of the potential of subwavelength technology for space instrument application.

References

1 Tetaz N., Ruilier C., Taccola M., Viard T., Lee Bouhours M.-S.L., Loiseaux B., Lehoucq G. (2017) Advanced large FOV UV/VIS/NIR/SWIR spectrometers for future earth observation instruments, *Proc. SPIE* **10563**, 1056333.
2 Ebstein S.M. (2001) Achromatic diffractive optical elements, *SPIE* **2404**, 211–216.
3 Kleemann B.H., Seesselberg M., Ruoff J. (2008) Design concepts for broadband high-efficiency DOEs, *J. Eur. Opt. Soc.* **3**, 08015.
4 Sandfuchs O., Kraus M., Brunner R. (2020) Structured metal double-blazed dispersion grating for broadband spectral efficiency achromatization, *J. Opt. Soc. Am. A* **37**, 1369–1380.
5 Mouroulis P., Wilson S.W., Maker P.D., Muller R.E. (1998) Convex grating types for concentric imaging spectrometers, *Appl. Opt.* **37**, p7200–7208.

6 Van Gorp B., Mouroulis P., Wilson D.W., Green R.O. (2014) Design of the compact wide swath imaging spectrometer (CWIS), *Proc. SPIE* **9222**, 92220C.

7 Sauvan C., Lalanne P., Lee M.-S.L. (2004) Broadband blazing with artificial dielectrics, *Opt. Lett.* **29**, 1593–1595.

8 Ribot C., Lee M.-S.L., Collin S., Bansropun S., Plouhinec P., Thenot D., Cassette S., Loiseaux B., Lalanne P. (2013) Broadband and efficient diffraction, *Adv. Opt. Mat.* **1**, p489–493.

9 Burmeister F., Flügel-Paul T., Zeitner U.D., Lee-Bouhours M.-S.L., Lehoucq G., Cholet J., Loiseaux B., Tetaz N., Windpassinger R., Taccola M. (2019) Binary blazed reflection grating for UV/VIS/NIR/SWIR spectral range, *Proc. SPIE* **11180**, 111801J.

10 Erdmann M., Kley E.-B., Zeitner U. (2017) Development of a large blazed transmission grating by effective binary index modulation for the GAIA radial velocity spectrometer, *Proc. SPIE* **105650**, 105651N.

11 Stork W., Streibl N., Haidner H., Kipfer P. (1991) Artificial distributed-index media fabricated by zero-order gratings, *Opt. Let.* **16**, 1921–1923.

12 Heusinger M., Banasch M., Flügel-Paul T., Zeitner U.D. (2016) Investigation and optimization of Rowland ghosts in high efficiency spectrometer gratings fabricated by e-beam lithography, *Proc. SPIE* **9759**, 97590A.

13 Wilson D.W., Maker P.D., Muller R.E., Mouroulis P.Z., Backlund J. (2003) Recent advances in blazed grating fabrication by electron-beam lithography, *Proc. SPIE* **5173**, 51730E.

14 Wilson D.W., Muller R.E., Echternach P.M., Backlund J.P. (2005) Electron-beam lithography for micro and nano-optical applications, *Proc. SPIE* **5720**, 68–77.

15 Zamkotsian F., Zhurminsky I., Lanzoni P., Tchoubaklian N., Lütolf F., Schnieper M., Schneider C., Fricke S., Fouchier M., Zerrad M., Amra C., Costes V., Loesel J. (2021) Blazed gratings on convex substrates for high throughput spectrographs for Earth and Universe observation, *Proc. SPIE* **11852**, 118520N.

16 Flügel-Paul T., Rothhardt C., Benkenstein T., Grabowski K., Risse S., Eberhardt R., Guldimann B., Zeitner U.D. (2018) All-dielectric Prism-Grating-Prism component realized by direct hydrophilic bonding technology for optical applications in space, *Proc. SPIE* **11180**, 1118014.

17 Birckigt P., Grabowski K., Leibeling G., Flügel-Paul T., Heusinger M., Ouslimani H., Risse S. (2021) Effects of static load and residual stress on fused silica direct bonding interface properties, *Appl. Phys. A* **127**, 938.